

See discussions, stats, and author profiles for this publication at: <https://www.researchgate.net/publication/263946409>

# Impact of Antidot Structure on the Multiradical Characters, Aromaticities, and Third-Order Nonlinear Optical Properties of Hexagonal Graphene Nanoflakes

ARTICLE *in* THE JOURNAL OF PHYSICAL CHEMISTRY C · AUGUST 2012

Impact Factor: 4.77 · DOI: 10.1021/jp305171k

---

CITATIONS

24

READS

8

## 8 AUTHORS, INCLUDING:



Kyohei Yoneda

Nara National College of Technology

42 PUBLICATIONS 599 CITATIONS

[SEE PROFILE](#)



Masayoshi Nakano

Osaka University

337 PUBLICATIONS 4,781 CITATIONS

[SEE PROFILE](#)



Yasuteru Shigeta

University of Tsukuba

174 PUBLICATIONS 1,836 CITATIONS

[SEE PROFILE](#)



Benoît Champagne

University of Namur

401 PUBLICATIONS 8,733 CITATIONS

[SEE PROFILE](#)

# Impact of Antidot Structure on the Multiradical Characters, Aromaticities, and Third-Order Nonlinear Optical Properties of Hexagonal Graphene Nanoflakes

Kyohei Yoneda, Masayoshi Nakano,\* Yudai Inoue, Tomoya Inui, Kotaro Fukuda, and Yasuteru Shigeta

Department of Materials Engineering Science, Graduate School of Engineering Science, Osaka University, Toyonaka, Osaka 560-8531, Japan

Takashi Kubo

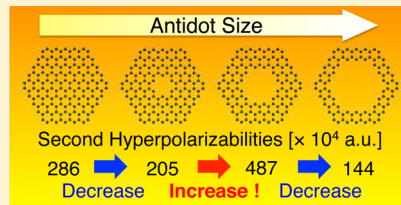
Department of Chemistry, Graduate School of Science, Osaka University, Toyonaka, Osaka 560-0043, Japan

Benoît Champagne

Laboratoire de Chimie Théorique (LCT), Facultés Universitaires Notre-Dame de la Paix (FUNDP), Rue de Bruxelles, 61, B-5000 Namur, Belgium

## S Supporting Information

**ABSTRACT:** The long-range corrected spin-unrestricted density functional theory, LC-UCLYP, method has been employed to unravel the relationship between the hole (referred to as “antidot”) structure of hexagonal graphene nanoflakes (HGNFs) and their properties, including their multiradical characters  $y_i$  [the occupation number of the lowest unoccupied natural orbital (LUNO) $+i$  ( $i = 0, 1, \dots$ )], aromaticity, and the second hyperpolarizabilities ( $\gamma$ ), which is the third-order nonlinear optical (NLO) response at the molecular level. These systems exhibit a wide range of open-shell/multiradical character, which shows an oscillatory behavior as a function of increasing the size of the antidot. This structural dependence is shown to originate from the oscillatory variations in the HOMO–LUMO energy gap, which result from the fact that the bonding and antibonding interactions between the central antidot-shape HGNFs and the surroundings alternate in both the HOMO and the LUMO as going from the center of the molecule to the peripheral region. Moreover, the multiradical character of these structures is strongly correlated with the variations of magnetic criteria of aromaticity, the nucleus-independent chemical shift (NICS) and the out-of-plane diagonal component of the magnetic shielding tensor ( $-\sigma_{zz}$ ), as well as with the  $\gamma$ . So, systems with larger multiradical characters tend to exhibit larger NICS and  $-\sigma_{zz}$  values, i.e., less aromaticity. Although the number of  $\pi$  electrons of the antidot HGNFs is smaller than that of the corresponding perfect  $C_{150}H_{30}$  HGNF, their  $\gamma$  value can be larger as evidenced by the antidot  $C_{126}H_{42}$  HGNF, which has intermediate multiradical characters ( $y_0 = y_1 = 0.658$ ) and displays a  $\gamma$  value 1.7 times larger than that of the perfect HGNF. These strong impacts of the antidot structure on the third-order NLO properties indicate that the antidot HGNFs are promising building blocks for a new class of multiradical NLO materials, the properties of which can be controlled by adjusting the antidot size.



## 1. INTRODUCTION

Over the past few years, a huge number of experimental and theoretical studies on graphene-like materials including two-dimensional (2D) graphenes, one-dimensional (1D) graphene nanoribbons (GNRs), and zero-dimensional (0D) graphene nanoflakes (GNFs) have been performed by chemists and physicists due to their unique electronic and spin properties, which are crucial for a wide range of applications in future electronics, spintronics, and photonics.<sup>1–3</sup> Owing to their honeycomb structures, low-dimensional nanographenes such as GNFs and GNRs have two types of edges, i.e., armchair and zigzag edges, the difference of which has a great influence on their electronic structures. Indeed, it is known that the more reactive  $\pi$  electrons tend to be localized on the zigzag edges<sup>4</sup>

and that, within single-determinant schemes [Hartree–Fock (HF) and density functional theory (DFT)], these GNFs present an open-shell singlet ground state, described by a spin-polarized broken-symmetry or spin-unrestricted solution. A key characteristic of these systems is their diradical or multiradical character, which is directly related to the open-shell nature described by the natural orbitals occupation numbers (except when they amount to 0 or 2). Since the diradical character is predicted to be at the origin of their unique physicochemical properties,<sup>3–11</sup> lots of studies have addressed the mechanism of

Received: May 28, 2012

Revised: July 29, 2012

Published: August 1, 2012



ACS Publications

© 2012 American Chemical Society

17787

dx.doi.org/10.1021/jp305171k | J. Phys. Chem. C 2012, 116, 17787–17795

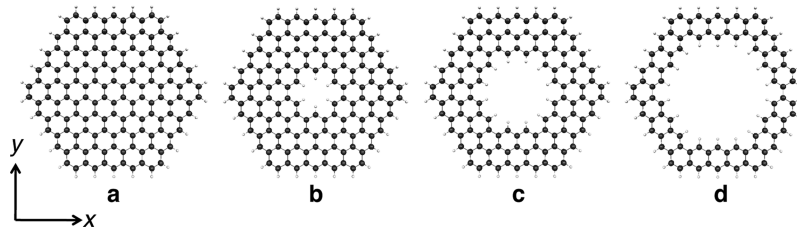


**Figure 1.** Structures of HGNFs with/without antidot structures,  $C_{150}H_{30}$  (**a**),  $C_{144}H_{36}$  (**b**),  $C_{126}H_{42}$  (**c**), and  $C_{96}H_{48}$  (**d**) and their coordinate axes. Carbon and hydrogen atoms are represented by dark and white circles, respectively.

the emerging open-shell character as well as on its control by chemical modifications<sup>10,12,13</sup> or physical perturbations.<sup>14</sup> On the other hand, the diradical character has been investigated from the viewpoint of the instability of the “chemical bond”,<sup>15</sup> e.g., along the dissociation process the diradical character ( $y$ ) (well-defined in quantum chemistry) of a diatomic molecule increases. For several singlet molecules, within single-determinant schemes, the ground state is, instead of closed-shell, open-shell with intermediate diradical characters.<sup>16</sup> For instance, calculations have predicted that zigzag-edged GNFs can exhibit intermediate and large  $y$  values, whereas the GNFs with mostly armchair edges present negligible diradical characters, which means these are nearly closed-shell systems.<sup>13b,d</sup> In addition, GNFs are expected to display not only diradical but also multiradical characters when their size increases.<sup>13d,e</sup>

In our recent studies, we have investigated several singlet diradical systems as a novel class of highly efficient nonlinear optical (NLO) molecules, which are fundamental materials for future photonics technologies such as optical switching, three-dimensional memory, optical limiting and photodynamic therapy.<sup>2b,17</sup> In the past, experimental and theoretical studies have revealed structure–NLO property relationships, highlighting several tuning parameters such as  $\pi$ -conjugation length, the intensity of the donor/acceptor substituents, and the charge.<sup>18,19</sup> However, most of these studies have been limited to closed-shell systems. In recent years, we have theoretically found that there exists an unexplored fertile field of open-shell NLO systems, which outstrip conventional closed-shell NLO systems in the performance and tunability. In particular, the second hyperpolarizability  $\gamma$ , the molecular property at the origin of the third-order NLO responses, exhibits a remarkable diradical character dependence: the systems with intermediate diradical characters show a large enhancement of  $\gamma$  as compared to closed-shell and pure diradical counterparts of similar size<sup>20,21</sup> as well as a giant electric field effect on  $\gamma$ .<sup>20e,f</sup> The mechanism of this enhancement has been clarified using analytical expressions derived from a two-site valence configuration interaction (VCI) scheme.<sup>20b–e</sup> This result has been exemplified using highly accurate ab initio molecular orbital (MO) and DFT calculations for various model and real open-shell molecular systems including GNFs.<sup>20a–c,21</sup> Subsequently, the diradical character dependence of  $\gamma$  has been confirmed experimentally by the incredibly huge two-photon absorption cross sections (a typical third-order NLO property) of several polyaromatic diphenalenyl diradicals,<sup>22</sup> which are thermally stable diradical systems and are predicted to possess intermediate  $y$  values. On the basis of these results, we have demonstrated that zigzag-edged GNFs exhibit enhanced  $\gamma$  values and a unique size dependence of  $\gamma$  due to their multiradical characters.<sup>13a–d</sup> It has also been found that the linear GNFs composed of trigonal units show different

multiradical characters and  $\gamma$  values depending on their linked forms, the results of which indicate that controlling the diradical character goes beyond the dependences upon the edge shape and size.<sup>13e</sup> Furthermore, recent progress in organic syntheses and physical fabrication of zigzag-edged GNFs with several shapes and sizes<sup>9,16d,e,23</sup> sheds light on the possibility of GNFs as highly promising and intriguing target compounds for future photonics and optoelectronics devices.

The open-shell character of a molecule has been associated with its aromaticity.<sup>24</sup> Since the diradical character is defined by the weight of the doubly excited configuration in the singlet ground state,<sup>15</sup> it evolves inversely to the energy gap between the highest occupied molecular orbital (HOMO) and the lowest unoccupied molecular orbital (LUMO). Therefore, antiaromatic or weakly aromatic systems, which possess near-degenerate electronic states, are expected to show large diradical characters. In a previous study,<sup>25</sup> we have elucidated the relationship between the aromaticity/antiaromaticity and the diradical character by comparing the results of polyacenes and dicyclopenta-fused acenes. These results suggest the possibility of an alternative control scheme of the NLO properties based on the aromaticity/antiaromaticity, which is one of the well-known chemical concepts.

In the present study, therefore, we investigate the impact of the molecular structure on the open-shell/multiradical character, the aromaticity/antiaromaticity, and the third-order NLO property in zigzag-edged hexagonal GNFs (HGNFs)<sup>13b</sup> with a fixed HGNF size but with varying the size of the hole, which are referred to as “antidot” structures. Although Hajgató et al. have reported that the aromaticity of HGNFs varies strongly depending on the size of antidot,<sup>26</sup> they have employed spin-restricted single-determinant schemes, assuming that the target molecules have no diradical character. Judging from the relationship between the open-shell character and the aromaticity/antiaromaticity as well as from their impacts on the optical and spin properties,<sup>24,25</sup> this study is extended here by considering spin-unrestricted solutions. To this end, we investigate the effects of the size of the antidot structure on the multiradical characters, the aromaticity/antiaromaticity, and the  $\gamma$  values of HGNFs using the long-range corrected UDFT, LC-UBLYP, method.<sup>27</sup> The present study contributes to a better understanding of the relationship among the multiradical characters, the aromaticities, and the structures in GNFs and thus to a construction of novel guidelines for designing highly efficient third-order NLO materials based on multiradical GNFs.

## 2. COMPUTATIONAL METHODS

### 2.1. Model Systems and Geometry Optimizations.

Figure 1 shows the molecular structures of perfect HGNF  $C_{150}H_{30}$  (**a**) and three antidot HGNFs, i.e.,  $C_{144}H_{36}$  (**b**),

$C_{126}H_{42}$  (**c**), and  $C_{96}H_{48}$  (**d**), where each outer zigzag edge is composed of 5 fused-rings. The antidot structures of molecules **b–d** take the shapes of benzene, coronene, and HGNF with three fused-rings per edge, respectively. The geometries of these systems were optimized by the spin-unrestricted (U) B3LYP/6-31G\* method under the constraint of  $D_{6h}$  symmetry. For molecules **a**, **b**, and **d**, the UB3LYP/6-31G\* solutions reduce to the spin-restricted (R) B3LYP/6-31G\* ones. These stable structures are also justified by the previous study by Hajgató et al.,<sup>26b</sup> which shows that the  $D_{6h}$  structures are the most stable for all of these systems at the B3LYP/6-31G level of approximation.

**2.2. Multiradical Character and Aromaticity.** The electronic structure of these systems, the instability of their chemical bonds, is characterized by multiple diradical characters  $y_i$ .<sup>15d</sup> Within single-determinant schemes, the  $y_i$  values [related to the highest occupied natural orbital (HONO)-*i* and the lowest unoccupied natural orbital (LUNO)+*i*, where *i* = 0, 1, ...] are defined by the occupation numbers ( $n_k$ ) of the natural orbitals (NOs)

$$y_i = n_{\text{LUNO}+i} = 2 - n_{\text{HONO}-i} \quad (1)$$

which range from 0 (closed-shell) to 1 (pure diradical), though the first equality of eq 1 can be employed for more general multi-determinant schemes.<sup>15d</sup>

We employed the LC-UBLYP/6-31G\* method with a range separating parameter  $\mu = 0.33$  to calculate the diradical characters, because it was shown to reproduce semiquantitatively the (hyper)polarizabilities of several open-shell molecules calculated using strongly electron-correlated *post-UHF* methods, e.g., the spin-unrestricted coupled cluster method including single and double excitations with a perturbative treatment of the triple excitations [UCCSD(T)].<sup>28</sup> The LC-UBLYP exchange-correlation functional is also reliable for the evaluation of the (hyper)polarizabilities of large size  $\pi$ -conjugated molecules as demonstrated in a recent investigation on the size dependences of the polarizability and the second hyperpolarizability in polyacetylenes and hydrogen chains as compared to other conventional functionals such as B3LYP.<sup>29</sup> Spin projected diradical characters, usually evaluated using UHF NO (UNO) occupation numbers,<sup>15b,d,30</sup> were also calculated for comparison, though spin contamination is generally smaller in the UDFT solutions than in the UHF ones. The antidot HGNFs present two identical diradical characters,  $y_0 = y_1$ , which originate from the same occupation numbers of their degenerate orbital pairs (HONO)-(HONO-1) [and of (LUNO)-(LUNO+1)] owing to their symmetries.

In order to address the aromaticity, we employed the nucleus-independent chemical shifts (NICS) calculated by the LC-UBLYP/6-31G\* method with gauge-independent atomic orbital (GIAO) approach.<sup>31</sup> The NICS value is defined as the negative value of the isotropic magnetic shielding constant

$$\text{NICS} = -\frac{1}{3}(\sigma_{xx} + \sigma_{yy} + \sigma_{zz}) \quad (2)$$

where  $\sigma_{ij}$  represents the *ij* component of the magnetic shielding tensor. The NICS values are specifically calculated 1 Å above the center-of-mass position of all six-membered rings, where  $\pi$ -electron contributions are expected to be dominant.<sup>32</sup> These NICS values are referred to as NICS(1Å) values. In addition, the out-of-plane diagonal  $-\sigma_{zz}(1\text{\AA})$  component has also been investigated since it is the component of NICS that is influenced by the magnetic field-induced ring currents in the

$\pi$ -electron clouds.<sup>33</sup> Indeed, there are examples demonstrating that, contrary to  $-\sigma_{zz}(1\text{\AA})$  values, the isotropic NICS fail in describing the magnetic aromaticity of molecules, including cyclopropane.<sup>34</sup> Thus, rings with large negative NICS(1Å) [or more precisely large negative  $-\sigma_{zz}(1\text{\AA})$ ] values are considered to be aromatic: generally the more negative the NICS(1Å) values, the more aromatic the rings are. In contrast, nonaromatic species have NICS(1Å) values close to zero and positive NICS(1Å) values are indicative of antiaromaticity. In addition, the NICS(1Å) and  $-\sigma_{zz}(1\text{\AA})$  values should be considered as qualitative descriptors of magnetic aromaticity rather than quantitative indices of magnetotropism, contrary to the derivative of the magnetic field-induced current, which is independent of the molecular geometry.<sup>35</sup> The LC-UBLYP method was found to well reproduce the experimental results on the relative chemical shifts in a singlet diradicaloid, pentalenol[1,2,3-*cd*;4,5,6-*c'd'*]diphenalene (PDPL), as compared to the LC-RBLYP results (see Figure S1 in the Supporting Information).

**2.3. Calculation and Analysis of  $\gamma$ .** Owing to the extended planar nature of the HGNFs and to their  $D_{6h}$  symmetry, just one diagonal tensor component has to be evaluated because the in-plane components dominate the orientationally averaged  $\gamma$  and because, by symmetry,  $\gamma_{xxxx} = \gamma_{yyyy} = 3\gamma_{xxyy}$ .<sup>36</sup> The LC-UBLYP/6-31G\* method is also employed for the calculation of  $\gamma$  values, in combination with the finite field (FF) approach,<sup>37</sup> which consists in the fourth-order numerical differentiation of the energy with respect to the applied external electric field. The field amplitudes are chosen so as to achieve a numerical accuracy within 1% error of the  $\gamma_{iiii}$  values. The  $\gamma$  density analysis<sup>38</sup> is applied to the elucidation of the spatial electronic contributions to  $\gamma$ . The  $\gamma$  density  $\rho_{iii}^{(3)}(\mathbf{r})$  is numerically calculated from the third-order derivative of the electron density with respect to the applied electric field

$$\rho_{iii}^{(3)}(\mathbf{r}) = \left. \frac{\partial^3 \rho}{\partial F_i \partial F_i \partial F_i} \right|_{F=0} \quad (3)$$

Using this density,  $\gamma$  is obtained by

$$\gamma_{iiii} = -\frac{1}{3!} \int r_i \rho_{iii}^{(3)}(\mathbf{r}) \, d\mathbf{r} \quad (4)$$

where  $r_i$  denotes the *i* component of the position vector. Positive and negative values of  $\rho_{iii}^{(3)}(\mathbf{r})$  multiplied by  $F^3$  correspond respectively to the field induced increase and decrease in the electron density (in proportion to  $F^3$ ), which induce the third-order dipole moment (third-order polarization) in the direction from positive to negative  $\gamma$  densities. For a pair of  $\rho_{iii}^{(3)}(\mathbf{r})$  distributions with positive and negative values, the contribution to  $\gamma_{iiii}$  is positive when the direction from the positive to negative  $\rho_{iii}^{(3)}(\mathbf{r})$  distribution coincides with the *i*-axis. The amplitude of the contribution of this pair of  $\rho_{iii}^{(3)}(\mathbf{r})$  is proportional to the distance between them. In the following sections,  $\gamma_{xxxx} = \gamma_{yyyy}$  are referred to as  $\gamma$ . All calculations were performed using the Gaussian 09 program packages.<sup>39</sup>

### 3. RESULTS AND DISCUSSION

**3.1. Diradical Character and Spin Density Distribution.** The diradical characters ( $y_0 = y_1$ ) are listed in Table 1. In the singlet ground states, molecules **a**, **b**, and **c** display nonzero diradical characters, while only molecule **d** displays a zero diradical character and therefore a closed-shell ground state. As

**Table 1. Diradical Characters  $y_0$  ( $=y_1$ )<sup>a</sup>, HOMO–LUMO Energy Gap ( $\Delta\epsilon \equiv \epsilon_{\text{LUMO}} - \epsilon_{\text{HOMO}}$ ) [eV], and the Second Hyperpolarizabilities ( $\gamma$ ) [ $\times 10^4$  a.u.] for Singlet HGNFs with/without Antidot Structures a–d Calculated Using the LC-UBLYP/6-31G\*( $\mu=0.33$ ) Method**

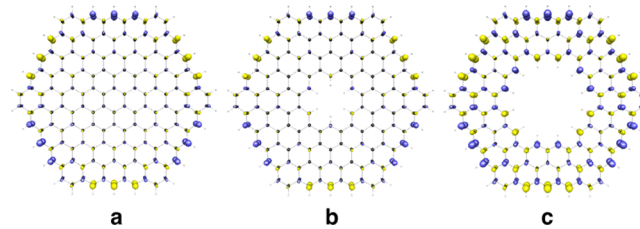
molecule	$y_0$ ( $=y_1$ )	$\Delta\epsilon$	$\gamma$
a	0.315 (0.208) <sup>b</sup>	3.994	286 (175) <sup>b</sup>
b	0.180 (0.130) <sup>b</sup>	4.703	205 (145) <sup>b</sup>
c	0.658 (0.474) <sup>b</sup>	2.735	487 (252) <sup>b</sup>
d	0.000 (0.034) <sup>b</sup>	6.221	144 (117) <sup>b</sup>

<sup>a</sup>The diradical characters are calculated from the NO occupation numbers. <sup>b</sup>The values in parentheses are obtained by the ASP-LC-UBLYP/6-31G\*( $\mu=0.47$ ) method.

compared to molecule a ( $y_0 = y_1 = 0.315$ ), molecule b with a benzene-shape antidot exhibits small diradical characters (0.180), whereas molecule c, having a larger antidot structure (coronene), shows large diradical characters (0.658). This oscillatory behavior of  $y_i$  as a function of the antidot size seems strange at first glance because open-shell singlet systems with larger  $\pi$ -conjugated domain tend to possess larger diradical characters.<sup>11,13b</sup> In addition, the  $y_2$  values are also nonzero except for molecule d, i.e.,  $y_2 = 0.200$  for a, 0.141 for b, and 0.341 for c. Since for each compound (a–c),  $y_2 < y_0 = y_1$ , the impact of  $y_2$  on  $\gamma$  is expected to be smaller and the  $y_2$  are not further discussed.

Before going ahead, it is worthwhile to address the spin contamination effects on the diradical characters and  $\gamma$  values since they can lead to incorrect results, e.g., the singlet–triplet energy gaps.<sup>40</sup> Nevertheless, these contamination effects depend on the exchange-correlation functionals in the UDFT method,<sup>41,42</sup> while they can also be corrected, e.g., by approximate spin projection schemes.<sup>15b,30</sup> For instance, when combining the perfect-pairing-type approximate spin projection (ASP) scheme<sup>15d</sup> with the LC-UBLYP XC functional [ASP-LC-UBLYP( $\mu=0.47$ )] the diradical character dependence of  $\gamma$  for a model diradical molecule, *p*-quinodimethane, reproduces well calculations performed with the strongly electron-correlated spin-unrestricted coupled cluster singles, doubles and perturbative triples [UCCSD(T)] method.<sup>41</sup> Note also that for the H<sub>4</sub> model compound, the UCCSD(T) scheme is adequate to reproduce the full CI results.<sup>43</sup> It has also been predicted that the non-spin-projected LC-UBLYP( $\mu=0.33$ ) can quantitatively reproduce the  $\gamma$  amplitudes [UCCSD(T)] in the intermediate and large diradical character regions, while the ASP-LC-UBLYP( $\mu=0.47$ ) give somewhat smaller  $\gamma$  amplitudes in those regions. Results on the antidot structures confirm these trends (Table 1) since the ASP-LC-UBLYP( $\mu=0.47$ ) and LC-UBLYP( $\mu=0.33$ )  $\gamma$  values evolve similarly as a function of the diradical character [ $y_0 (= y_1)$ ]. The decrease in the diradical character for a–c originates from the removal of spin contaminations but its ordering remains d < b < a < c. Note that due to the larger  $\mu$  value, the LC-UBLYP( $\mu=0.47$ ) method attributes a small diradical character to d in contrast to the  $\mu = 0.33$  case whereas the ASP-LC-UBLYP( $\mu=0.47$ )  $\gamma$  amplitudes are smaller than the LC-UBLYP( $\mu=0.33$ ) ones. On the basis of these results, the LC-UBLYP( $\mu=0.33$ ) method is relevant for predicting relative  $\gamma$  values of antidot systems and for analyzing them and therefore most of our analysis is carried out at that level of approximation.

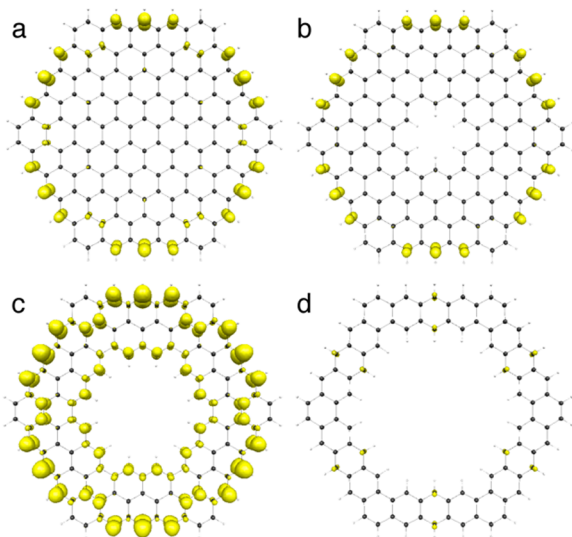
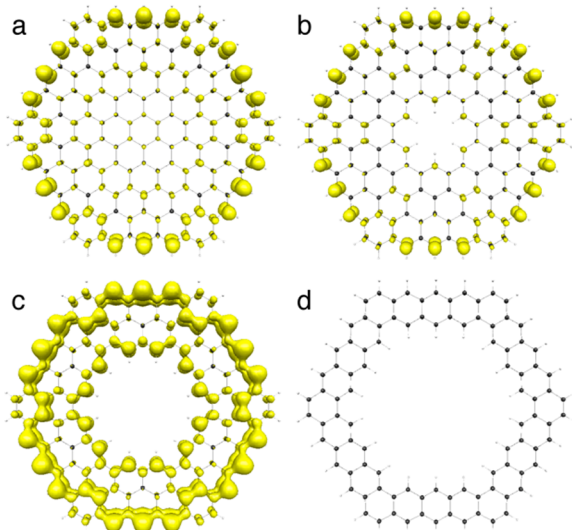
Figure 2 shows the spin density distributions of a, b, and c in their singlet ground states. Although the spin polarization,



**Figure 2.** Spin density distributions in singlet HGNFs with/without antidot structures a–c (Figure 1) calculated using the LC-UBLYP/6-31G\* method. The yellow and blue surfaces represent  $\alpha$  and  $\beta$  spin densities with  $\pm 0.015$  a.u. iso-surfaces, respectively.

originating from the broken-symmetry single-determinant approach, is not experimentally observable in singlet systems, it is useful for analyzing the spatial correlation between the  $\alpha$  and  $\beta$  spins.<sup>11,15b,d</sup> Indeed, the relative odd electron density distributions,<sup>15d</sup> obtained from the NOs and their occupation numbers and representing the spatial contributions of the odd electrons to the multiradical characters, calculated at the ASP-LC-UBLYP( $\mu=0.47$ ) and the LC-UBLYP( $\mu=0.33$ ) levels of approximation are in good agreement with those obtained from LC-UBLYP( $\mu=0.33$ ) spin density distributions except for the sign of spin densities (see Figures 2 and 3, as well as the Supporting Information). Namely, the amplitude of the spin polarization reflects that of the diradical character: the spin density amplitudes of c (having the largest diradical characters among these molecules) are larger than those of the others, whereas those of a are slightly larger than those of b. The primary spin densities (i) are localized on the middle of the outer zigzag edges, with sign alternation between adjacent edges (though spin polarization is also observed between adjacent carbon atoms on each edge) and (ii) rapidly decrease with the distance from the outer edge regions. For the antidot HGNFs b and c, the next primary spin densities are observed on the inner zigzag edges, which have spin densities with opposite sign and smaller amplitudes than on the outer edges.

Considering its definition, the origin of the antidot size dependence of the diradical characters should be connected to the energy gap variations, and thereof to the topology of the MOs. For all systems and their moieties, we focus on the HOMO–LUMO energy gaps and the corresponding MOs determined at the LC-RBLYP/6-31G\* level (see Figure 4). Note that unlike for other properties we discuss the HOMO–LUMO gaps based on spin-restricted calculations because, within spin-restricted schemes such as RHF and RDFT, the diradical character is defined by twice the weight of the doubly excited configuration in the singlet ground state (e.g., from HOMO to LUMO in the case of  $y_0$ , which also represents the magnitude of the static correlation between the HOMO and the LUMO).<sup>15a,b,20b</sup> This choice is also supported by the fact that, for the a–c open-shell systems the UNOs obtained using the LC-UBLYP method are similar to the RNOs or the spin-restricted canonical molecular orbitals (RMOs). The discussion only considers one set of degenerate frontier orbitals but an equivalent analysis can be performed using the HOMO-1/LUMO+1 (shown in Figure S2 in the Supporting Information). Results listed in Table 1 supports the relationship where smaller HOMO–LUMO gaps ( $\Delta\epsilon$ ) lead to larger diradical characters. The larger gap in b (4.703 eV) with respect to a

ASP-LC-UBLYP( $\mu=0.47$ )/6-31G\*LC-UBLYP( $\mu=0.33$ )/6-31G\*

**Figure 3.** Odd electron density distributions (with contour 0.001) of HGNFs **a–d** calculated using the ASP-LC-UBLYP( $\mu=0.47$ )/6-31G\* and LC-UBLYP( $\mu=0.33$ )/6-31G\* methods.

(3.994 eV) results from both the stabilization of the HOMO and the destabilization of the LUMO, which result from the specific bonding and antibonding interactions between the central hexagonal ring (benzene) of molecule **a** and its surrounding, which corresponds formally to molecule **b**. Indeed, for the HOMO, these interactions are antibonding while there are bonding for the LUMO. Thus, going from **a** to **b** corresponds to the removal of the central hexagonal ring, which stabilizes the HOMO and destabilizes the LUMO. In contrast, the orbital distributions in **a** between the central moiety composed of 7 fused-rings (corresponding to a coronene molecule) and its surrounding (corresponding to a molecule **c**) point out to bonding interactions in the HOMO and to antibonding interactions in the LUMO. Thus, the removal of this central coronene from **a** destabilizes the HOMO, stabilizes the LUMO, and decreases the gap of **c** (2.735 eV).

On the other hand, the HOMO and LUMO of molecule **d** are obviously different from those of the three other molecules. In fact, the orbitals corresponding to the HOMO (LUMO) of the other molecules are much stabilized (destabilized) in **d** due to cutting away a large central moiety and they become HOMO-2 (LUMO+2). This stabilization (destabilization) of the HOMO-2 (LUMO+2) can also be understood from the orbital interactions starting from molecule **b**, having the largest  $\Delta\epsilon$  among **a–c**, where the antibonding (HOMO) or bonding (LUMO) interactions between the inner two carbon rings and the surrounding moiety are removed upon forming molecule **d**.

The bonding and antibonding interactions in the HOMO and LUMO of HGNFs, which alternate as going from the center to the periphery of the molecule, are further discussed by considering that these HGNFs are composed of [12n-6]annulenes ( $n = 1, 2, \dots$ ). It is found that (i) coronene is composed of benzene ( $n = 1$ ) and [18]annulene ( $n = 2$ ) (see Figure 5 for the orbital correlation diagram), (ii) the HOMO–LUMO gap of [18]annulene is smaller than that of benzene because of the larger number of  $\pi$ -conjugated electrons, (iii) there are one nodal plane in the HOMO and two nodal planes in the LUMO for benzene, whereas for [18]annulene, there are four and five in the HOMO and LUMO, respectively, (iv) the latter can be understood resorting to the Hückel theory: [12n-6]annulene is expected to exhibit  $3n-2$  nodes in the HOMO and  $3n-1$  nodes in the LUMO, and (v) the symmetry determines the allowed interactions between the LUMO of benzene ( $e_{2u}$ ) and the HOMO of [18]annulene to form the HOMO of coronene as well as between the HOMO of benzene ( $e_{1g}$ ) and the LUMO of [18]annulene to form the LUMO of coronene.

Next, we consider the interactions between coronene and [30]annulene ( $n = 3$ ), which formally construct a HGNF with three fused-ring per edge,  $C_{54}H_{18}$ . [30]annulene exhibits a smaller HOMO–LUMO gap than coronene and shows seven and eight nodes in the HOMO and LUMO, respectively, in which the odd–even sequence of node numbers is opposite to the coronene case [the even (HOMO) and odd (LUMO) numbers of nodal planes as mentioned in the previous paragraph]. The HOMO of  $C_{54}H_{18}$  is formed by a bonding interaction between the LUMO of coronene and the HOMO of [30]annulene, whereas the LUMO of  $C_{54}H_{18}$  is formed by an antibonding interaction between the HOMO of coronene and the LUMO of [30]annulene. Therefore, the interaction between the central benzene moiety and the surrounding in the HOMO(LUMO) of  $C_{54}H_{18}$  is antibonding(bonding) because the HOMO(LUMO) of  $C_{54}H_{18}$  involves the LUMO(HOMO) of coronene.

So, in the [12n-6]annulene family, the odd–even node numbers in the HOMO and LUMO alternate with  $n$ , in agreement with the Hückel theory. Consequently, considering the growing process of HGNFs, it can be predicted that, for any new HGNF, the HOMO is constructed from the HOMO of the annulene and the LUMO of the original HGNF, whereas the LUMO is done from the LUMO of the annulene and the HOMO of the original HGNF. As a result, in the HOMO and LUMO of the HGNFs, the bonding and antibonding interactions between the HGNF and the adjacent outer annulene alternate, which is at the origin of the unique antidot size dependence of the diradical characters of HGNFs.

**3.2. Aromaticity.** The LC-UBLYP/6-31G\* NICS(1Å) values on all of the six-membered rings of the HGNFs with/without antidot structures are listed in Table 2, where the ring

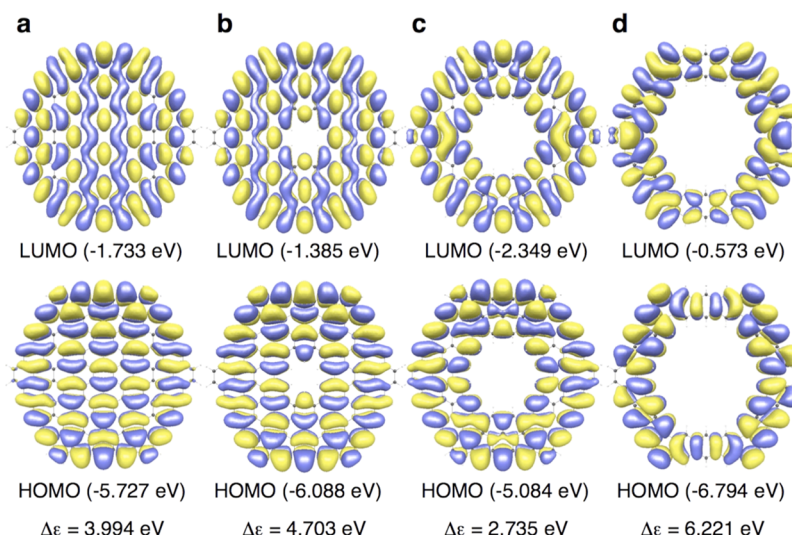


**Figure 4.** Molecular orbitals (MOs) and orbital energies of HGNFs with/without antidot structures **a–d** (Figure 1) calculated using the LC-RBLYP/6-31G\* method. The HOMO–LUMO energy gaps ( $\Delta\epsilon$ ) are also shown. The yellow and blue surfaces represent positive and negative MOs with  $\pm 0.007$  a.u. iso-surfaces, respectively.

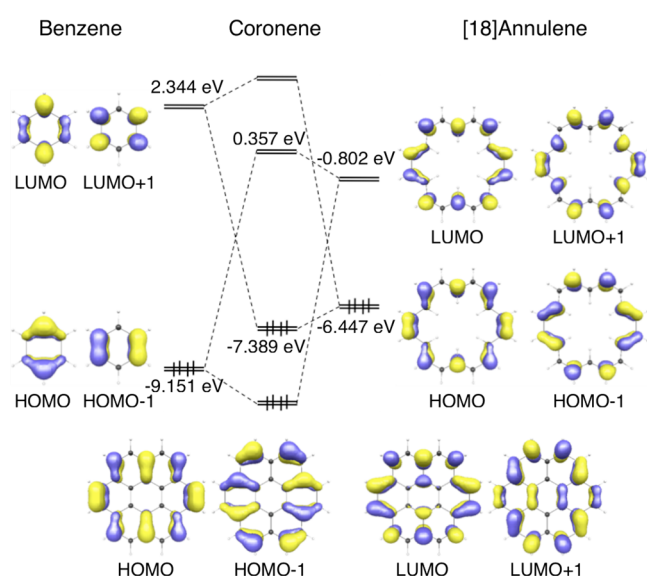


**Figure 5.** LC-RBLYP/6-31G\* orbital correlation diagram for coronene, which is assumed to be composed of benzene and [18]annulene. The yellow and blue surfaces represent positive and negative MOs with  $\pm 0.080$ ,  $\pm 0.050$ , and  $\pm 0.040$  a.u. iso-surfaces for benzene, [18]annulene, and coronene, respectively.

numbers are defined in Figure 6. As sketched in Figure 7, the larger the diradical character, the higher (less negative) the NICS( $1\text{\AA}$ ) values, and therefore, to some extent, the weaker the aromaticity. In particular, the NICS( $1\text{\AA}$ ) values for the closed-shell molecule **d** are clearly more negative than those of the

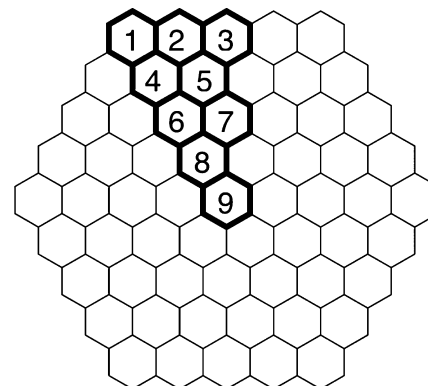


**Figure 6.** Numbering of the HGNF nonequivalent rings used for the NICS( $1\text{\AA}$ ) values listed in Table 2.

other molecules. Then, the NICS( $1\text{\AA}$ ) values in the middle of the outer zigzag edges (ring 3 in Figure 6), on which spin densities with large amplitudes are distributed (see Figure 2), increase in the order: **d** < **b** < **a** < **c**. This substantiates that the reduction of NICS( $1\text{\AA}$ ) amplitude is associated with the increase of diradical character. Also for the rings of the inner zigzag edges of the antidot structures, the NICS( $1\text{\AA}$ ) values are more negative when the spin density is smaller, as found when comparing ring 7 in molecule **b** and ring 5 in molecule **c**. This argument is however qualitative since the NICS( $1\text{\AA}$ ) value on the top of a given ring results from the magnetic field induced currents on that ring as well as on the surrounding rings. For instance, in molecule **b**, the NICS( $1\text{\AA}$ ) amplitude increases

**Table 2.** NICS( $1\text{\AA}$ ) Values [ppm] on Rings 1–9 (See Figure 6), and Average NICS( $1\text{\AA}$ ) Values per Ring (NICSav) [ppm] for HGNFs **a–d** with/without Antidot Structures Calculated Using the LC-UUBLYP/6-31G\* Method

molecule	1	2	3	4	5	6	7	8	9	NICSav
<b>a</b>	-2.04	-8.32	-10.7	-10.4	-6.93	-7.77	-10.1	-7.56	-9.92	-7.94
<b>b</b>	-2.00	-8.54	-12.1	-12.2	-4.91	-3.91	-11.0			-7.57
<b>c</b>	-5.79	-7.35	-6.66	-2.73	-8.67					-6.74
<b>d</b>	-2.76	-10.7	-13.3							-9.37

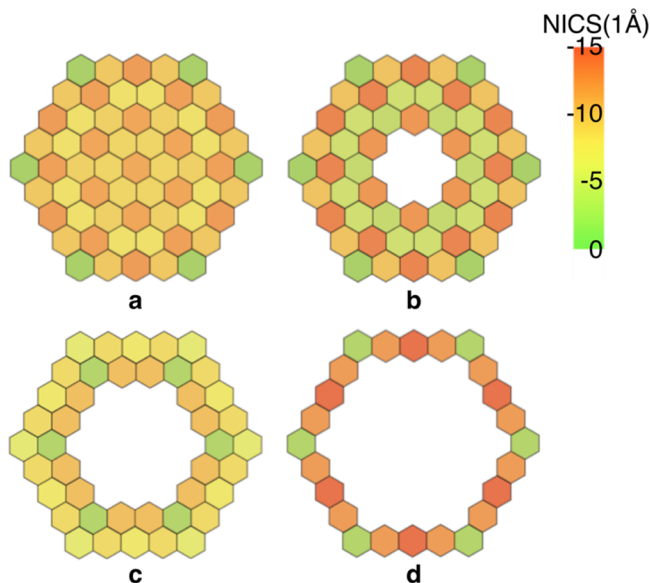


**Figure 7.** Colored maps for the NICS( $1\text{\AA}$ ) values [ppm] of HGNFs with/without antidot structures calculated using the LC-UBLYP/6-31G\* method.

from ring 1 to ring 3, whereas the largest spin density and therefore the largest open-shell character is localized on ring 3.

To a good extent, the average NICS( $1\text{\AA}$ ) values (NICSav), which provide a measure of the global aromaticity (Table 2) also correlate with the diradical character. A noticeable exception is the inversion between **a** and **b**: molecule **a** exhibits a slightly lower NICSav value ( $-7.94$  ppm) than molecule **b** ( $-7.57$  ppm) though molecule **a** has larger diradical characters (0.315) than molecule **b** (0.180). To assess the origin of this inversion, we have also examined the  $-\sigma_{zz}(1\text{\AA})$  values (see Table S1 and Figure S3 in the Supporting Information), but similar trends are observed. This certainly points out the fact that the NICSav values are global characteristics whereas the frontier orbitals are localized on parts of the molecule.

Much different NICS( $1\text{\AA}$ ) distributions are obtained when imposing a spin-restricted solution (Table S2 and Figure S4), which corresponds to another aromatic picture of molecules **a**–**d**, and to other linear and nonlinear optical properties. Indeed, the LC-RBLYP/6-31G\* ( $\mu=0.33$ ) method, overestimates the amplitude of the NICS( $1\text{\AA}$ ) and NICSav values and this overestimation increases with the diradical character. Therefore, for the NICSav values, the  $\mathbf{d} < \mathbf{a} < \mathbf{b} < \mathbf{c}$  ordering is modified into  $\mathbf{c} < \mathbf{a} < \mathbf{d} < \mathbf{b}$ . Though the absolute values are slightly different, similar trends were obtained with the RB3LYP/6-31G method.<sup>26b</sup> This comparison is consistent with previous investigations showing that (i) the NICS analysis with spin-restricted calculations cannot explain the high instabilities of large polyacenes,<sup>44</sup> whereas the LC-UBLYP approach accounts for their transverse spin polarization, their nonzero diradical characters, and their less negative NICS( $1\text{\AA}$ )<sup>25</sup> and (ii) the inner rings are more reactive as evidenced by the regioselectivity of the [4 + 2] cycloaddition of  $\text{C}_{60}$  with pentacene.<sup>45</sup>

**3.3. Second Hyperpolarizabilities.** We now examine the antidot structure dependence of the  $\gamma$  values in these HGNFs (Table 1). Molecule **c** shows the largest  $\gamma$  value ( $487 \times 10^4$  a.u.), whereas molecule **d** presents the smallest  $\gamma$  ( $144 \times 10^4$  a.u.). The  $\gamma$  values of molecules **a** ( $286 \times 10^4$  a.u.) and **b** ( $205 \times 10^4$  a.u.) lie in between those of molecule **c** and **d**. Since it is

well-known that in  $\pi$ -conjugated systems  $\gamma$  increases non-linearly with the  $\pi$ -delocalization length, the GNFs with antidot structures (**b**–**d**) are expected to possess smaller  $\gamma$  than the perfect HGNF (**a**) of the similar size. On the contrary, the  $\gamma$  value of molecule **c**, with intermediate diradical characters, is about 1.7 and 2.4 times as large as those of molecules **a** and **b**, with smaller diradical characters but larger number of C atoms, respectively. The smallest  $\gamma$  of molecule **d** results from the smallest  $\pi$ -conjugation size as well as from its closed-shell nature. Such a significant diradical character dependence of  $\gamma$  in these HGNFs is in good agreement with our previous results for open-shell NLO systems. Namely, the relative amplitude of  $\gamma$  for molecules **a**–**c** is governed by the diradical character and not by the  $\pi$ -conjugation size.

Figure 8 shows the  $\gamma$  density [ $\rho_{yy}^{(3)}(\mathbf{r})$ ] distributions of these HGNFs, which, for all systems, mostly originate from the  $\pi$

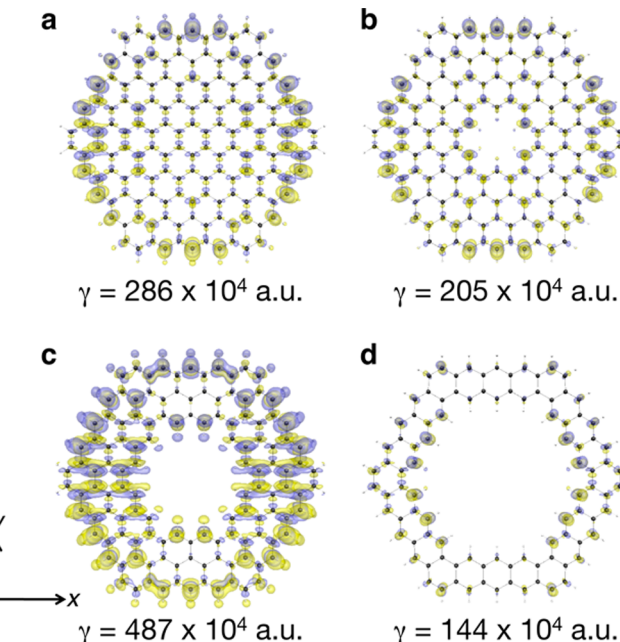


**Figure 8.**  $\gamma$  density [ $\rho_{yy}^{(3)}(\mathbf{r})$ ] distributions in singlet HGNFs with/without antidot structures as well as their  $\gamma$  values. The yellow and blue meshes represent positive and negative densities with  $\pm 900$  a.u. iso-surfaces, respectively.

electrons. It is found that the  $\rho_{yy}^{(3)}(\mathbf{r})$  amplitudes are the largest in molecule **c**, whereas those of molecule **d** are the smallest. Then, the  $\rho_{yy}^{(3)}(\mathbf{r})$  of molecules **a**–**c** are primarily distributed on the outer zigzag edges, on which the dominant spin densities are distributed (see Figure 2), and the dominant positive and negative densities are well separated and located on the bottom and upper sides, respectively, leading to positive  $\gamma$  values. In addition, for compounds **b** and **c**, non-negligible  $\rho_{yy}^{(3)}(\mathbf{r})$  amplitudes are present on the inner zigzag edges, leading to additional positive contributions to  $\gamma$ . On the other hand, the  $\rho_{yy}^{(3)}(\mathbf{r})$  of the closed-shell molecule **d** is distinct with negligible values on the top and bottom edges. These  $\rho_{yy}^{(3)}(\mathbf{r})$  distribution patterns and their amplitudes substantiate the relative  $\gamma$  values of these systems.

#### 4. SUMMARY

In this study, we have theoretically clarified the antidot structure dependences of the diradical characters, of some

magnetic criteria of aromaticity, and of the second hyperpolarizabilities ( $\gamma$ ) in hexagonal GNFs (HGNFs). It is found that the open-shell/diradical characters, which are larger in polyaromatic hydrocarbons with larger zigzag edges,<sup>11,13</sup> exhibit an oscillating behavior as a function of the size of the antidot structure. Furthermore, relationships between the NICS(1Å) and  $-\sigma_{zz}(1\text{\AA})$  values and the open-shell character have been observed, that is, the HGNFs with larger diradical characters tend to show less negative NICS(1Å) and  $-\sigma_{zz}(1\text{\AA})$  values, which corresponds to less aromaticity. These antidot structure dependences have been interpreted by the oscillatory variations in the HOMO–LUMO energy gap, which result from the fact that the bonding and antibonding interactions between the central antidot-shape HGNFs, i.e., the missing part of the HGNFs, and the surroundings alternate in both the HOMO and the LUMO as going from the center of the molecule to the peripheral region. Furthermore, this antidot size dependence of the HOMO and LUMO distributions has been unraveled on the basis of simple Hückel MO theory applied to the electronic structure of HGNFs, which are viewed as structures build from [12n-6]annulenes. In agreement with previous structure-NLO property relationships, the  $\gamma$  values exhibit a strong diradical character dependence in these antidot HGNFs. In particular, the  $\gamma$  value of the antidot C<sub>126</sub>H<sub>42</sub> HGNF with intermediate open-shell characters is about 1.7 times as large as that of the perfect HGNF despite of a 16% reduction in the number of  $\pi$  electrons. The present results reveal therefore that the antidot HGNFs are promising building blocks of a new class of highly efficient NLO materials with a novel tuning parameter, the antidot size, which greatly influences the diradical character and magnetic criteria of aromaticity.

## ASSOCIATED CONTENT

### Supporting Information

Chemical shifts  $\delta$  [ppm] of pentaleno[1,2,3-*cd*;4,5,6-*c'd'*] diphenalene (PDPL) calculated by the LC-U/RBLYP( $\mu=0.33$ ) methods. Molecular orbitals (MOs) of **a–d** calculated using the LC-RBLYP/6-31G\*. Values and colored maps of  $-\sigma_{zz}(1\text{\AA})$  and NICS(1Å) of **a–d** calculated by the LC-(R)UBLYP/6-31G\* methods. Definition of odd electron density and approximate spin projection scheme. This material is available free of charge via the Internet at <http://pubs.acs.org>.

## AUTHOR INFORMATION

### Corresponding Author

\*Fax: +81-6-6850-6268. E-mail: mnaka@cheng.es.osaka-u.ac.jp.

### Notes

The authors declare no competing financial interest.

## ACKNOWLEDGMENTS

This work is supported by Grant-in-Aid for Scientific Research (No. 21350011) from Japan Society for the Promotion of Science (JSPS), Grant-in-Aid for JSPS Fellows (No. 23-1632), and the global COE (center of excellence) program “Global Education and Research Center for Bio-Environmental Chemistry” of Osaka University. This work has also been supported by the Academy Louvain (ARC “Extended  $\pi$ -Conjugated Molecular Tinkertoys for Optoelectronics, and Spintronics”) and by the Belgian Government (IUAP N° P06-27 “Functional Supramolecular Systems”).

## REFERENCES

- (1) Novoselov, K. S.; Geim, A. K.; Morozov, S. V.; Jiang, D.; Zhang, Y.; Dubonos, S. V.; Grigorieva, V.; Firsov, A. A. *Science* **2004**, *306*, 666–669.
- (2) (a) Castro Neto, A. H.; Guinea, F.; Peres, N. M. R.; Novoselov, K. S.; Geim, A. K. *Rev. Mod. Phys.* **2009**, *81*, 109–162. (b) Du, A.; Smith, S. C. *J. Phys. Chem. Lett.* **2011**, *2*, 73–80.
- (3) (a) Son, Y. W.; Cohen, M. L.; Louie, S. G. *Nature* **2006**, *444*, 347–349. (b) Lambert, C. *Angew. Chem., Int. Ed.* **2011**, *50*, 1756–1758.
- (4) (a) Fujita, M.; Wakabayashi, K.; Nakada, K.; Kusakabe, K. *J. Phys. Soc. Jpn.* **1996**, *65*, 1920–1923. (b) Nakada, K.; Fujita, M.; Dresselhaus, G.; Dresselhaus, M. S. *Phys. Rev. B* **1996**, *54*, 17954–17961.
- (5) (a) Pisani, L.; Chan, J. A.; Montanari, B.; Harrison, N. M. *Phys. Rev. B* **2007**, *75*, 064418–1–9. (b) Vandescuren, M.; Hermet, P.; Meunier, V.; Henrard, L.; Lambin, Ph. *Phys. Rev. B* **2008**, *78*, 195401–1–8.
- (6) Dutta, S.; Pati, S. K. *J. Mater. Chem.* **2010**, *20*, 8207–8223.
- (7) Yazyev, O. V.; Wang, W. L.; Meng, S.; Kaxiras, E. *Nano Lett.* **2008**, *8*, 766–766.
- (8) (a) Ezawa, M. *Phys. Rev. B* **2007**, *76*, 245415–1–6. (b) Rossier, J.-F.; Palacios, J. *J. Phys. Rev. Lett.* **2007**, *99*, 177204–1–4.
- (9) (a) Yang, X.; Dou, X.; Rouhanipour, A.; Zhi, L.; Rader, H.; Müllen, K. *J. Am. Chem. Soc.* **2008**, *130*, 4216–4217. (b) Zhi, L. J.; Müllen, K. *J. Mater. Chem.* **2008**, *18*, 1472–1484. (c) Treier, M.; Pignedoli, C. A.; Laino, T.; Rieger, R.; Müllen, K.; Passerone, D.; Fasel, R. *Nat. Chem.* **2011**, *3*, 61–67.
- (10) Dias, J. R. *Chem. Phys. Lett.* **2008**, *467*, 200–203.
- (11) (a) Bendikov, M.; Duong, H. M.; Starkey, K.; Houk, K. N.; Carter, E. A.; Wudl, F. *J. Am. Chem. Soc.* **2004**, *126*, 7416–7417. (b) Hachmann, J.; Dorando, J. J.; Avilés, M.; Chan, G. K.-L. *J. Chem. Phys.* **2007**, *127*, 134309–1–9. (c) Chen, Z.; Jiang, D.-E.; Lu, X.; Bettinger, H. F.; Dai, S.; Schleyer, P. V. R.; Houk, K. N. *Org. Lett.* **2007**, *9*, 5449–5452. (d) Jiang, D.-E.; Dai, S. *J. Phys. Chem. A* **2008**, *112*, 332–335. (e) Tönshoff, C.; Bettinger, H. F. *Angew. Chem., Int. Ed.* **2010**, *49*, 4125–4128.
- (12) (a) Huang, B.; Liu, F.; Wu, J.; Gu, B.-L.; Duan, W. *Phys. Rev. B* **2008**, *77*, 153411. (b) Hod, O.; Barone, V.; Peralta, J. E.; Scuseria, G. E. *Nano Lett.* **2007**, *7*, 2295–2299.
- (13) (a) Nakano, M.; Nagai, H.; Fukui, H.; Yoneda, K.; Kishi, R.; Takahashi, H.; Shimizu, A.; Kubo, T.; Kamada, K.; Ohta, K.; et al. *Chem. Phys. Lett.* **2008**, *467*, 120–125. (b) Nagai, H.; Nakano, M.; Yoneda, K.; Fukui, H.; Minami, T.; Bonness, S.; Kishi, R.; Takahashi, H.; Kubo, T.; Kamada, K.; et al. *Chem. Phys. Lett.* **2009**, *477*, 355–359. (c) Yoneda, K.; Nakano, M.; Kishi, R.; Takahashi, H.; Shimizu, A.; Kubo, T.; Kamada, K.; Ohta, K.; Champagne, B.; Botek, E. *Chem. Phys. Lett.* **2009**, *480*, 278–283. (d) Nagai, H.; Nakano, M.; Yoneda, K.; Kishi, R.; Takahashi, H.; Shimizu, A.; Kubo, T.; Kamada, K.; Ohta, K.; Botek, E.; et al. *Chem. Phys. Lett.* **2010**, *489*, 212–218. (e) Yoneda, K.; Nakano, M.; Fukui, H.; Minami, T.; Shigeta, Y.; Kubo, T.; Ohta, K.; Botek, E.; Champagne, B. *ChemPhysChem* **2011**, *12*, 1697–1707.
- (14) (a) Kan, E.-J.; Li, Z.; Yang, J.; Hou, J. G. *Appl. Phys. Lett.* **2007**, *91*, 243116–1–3. (b) Sawada, K.; Ishii, F.; Saito, M. *Appl. Phys. Express* **2008**, *1*, 064004–1–3.
- (15) (a) Hayes, E. F.; Siu, A. K. Q. *J. Am. Chem. Soc.* **1971**, *93*, 2090–2091. (b) Yamaguchi, K. In *Self-Consistent Field: Theory and Applications*; Carbo, R., Klobukowski, M., Eds.; Elsevier: Amsterdam, 1990; pp 727–828. (c) Kamada, K.; Ohta, K.; Shimizu, A.; Kubo, T.; Kishi, R.; Takahashi, H.; Botek, E.; Champagne, B.; Nakano, M. *J. Phys. Chem. Lett.* **2010**, *1*, 937–940. (d) Nakano, M.; Fukui, H.; Minami, T.; Yoneda, K.; Shigeta, Y.; Kishi, R.; Champagne, B.; Botek, E.; Kubo, T.; Ohta, K.; et al. *Theor. Chem. Acc.* **2011**, *130*, 711–724. *erratum* **130**, 725–726. (e) Head-Gordon, M. *Chem. Phys. Lett.* **2003**, *372*, 508–511.
- (16) (a) Kubo, T.; Shimizu, A.; Uruichi, M.; Yakushi, K.; Nakano, M.; Shiomi, D.; Sato, K.; Takui, T.; Morita, Y.; Nakasui, K. *Org. Lett.* **2007**, *9*, 81–84. (b) Shimizu, A.; Uruichi, M.; Yakushi, K.; Matsuzaki, H.; Okamoto, H.; Nakano, M.; Hirao, Y.; Matsumoto, K.; Kurata, H.;

- Kubo, T. *Angew. Chem., Int. Ed.* **2009**, *48*, 5482–5486. (c) Huang, J.; Kertesz, M. *J. Am. Chem. Soc.* **2007**, *129*, 1634–1643. (d) Konishi, A.; Hirao, Y.; Nakano, M.; Shimizu, A.; Botek, E.; Champagne, B.; Shiomi, D.; Sato, K.; Takui, T.; Matsumoto, K.; et al. *J. Am. Chem. Soc.* **2010**, *132*, 11021–11023. (e) Tönshoff, C.; Bettinger, H. F. *Angew. Chem., Int. Ed.* **2010**, *49*, 4125–4128.
- (17) (a) Pathenopoulos, D. A.; Rentzepis, P. M. *Science* **1989**, *245*, 843–845. (b) Zhou, W.; Kuebler, S. M.; Braun, K. L.; Yu, T.; Cammack, J. K.; Ober, C. K.; Perry, J. W.; Marder, S. R. *Science* **2002**, *296*, 1106–1109. (c) Frederiksen, P. K.; Jørgensen, M.; Ogilby, P. R. *J. Am. Chem. Soc.* **2001**, *123*, 1215–1221.
- (18) (a) Slepkov, A. D.; Hegmann, F. A.; Eisler, S.; Elliott, E.; Tykwiński, R. R. *J. Chem. Phys.* **2004**, *120*, 6807–6810. (b) Terenziani, F.; Katan, C.; Badaeva, E.; Tretiak, S.; Blanchard-Desce, M. *Adv. Mater.* **2008**, *20*, 4641–4678. (c) Bouit, P. A.; Kamada, K.; Feneyrou, P.; Berginc, G.; Toupet, L.; Maury, O.; Andraud, C. *Adv. Mater.* **2009**, *21*, 1151–1154.
- (19) (a) Toto, J. L.; Toto, T. T.; de Melo, C. P.; Kirtman, B.; Robins, K. *J. Chem. Phys.* **1996**, *104*, 8586–8592. (b) Tretiak, S.; Chernyak, V.; Mukamel, S. *Phys. Rev. Lett.* **1996**, *77*, 4656–4659. (c) Oliveira, L. N.; Amaral, O. A. V.; Castro, M. A.; Fonseca, T. L. *Chem. Phys.* **2003**, *289*, 221–230. (d) Ferrighi, L.; Frediani, L.; Cappelli, C.; Salek, P.; Ågren, H.; Helgaker, T.; Ruud, K. *Chem. Phys. Lett.* **2006**, *425*, 267–272. (e) Limacher, P. A.; Mikkelsen, K. V.; Lüthi, H. P. *J. Chem. Phys.* **2009**, *130*, 194114–1–7. (f) Chen, W.; Yu, G.; Gu, F. L.; Aoki, Y. *Chem. Phys. Lett.* **2009**, *474*, 175–179. (g) Zein, S.; Delbecq, F.; Simon, D. *Phys. Chem. Chem. Phys.* **2009**, *11*, 694–702. (h) Zalesny, R.; Loboda, O.; Iliopoulos, K.; Chatzikyriacos, G.; Couris, S.; Rotas, G.; Tagmatarchis, N.; Avramopoulos, A.; Papadopoulos, M. G. *Phys. Chem. Chem. Phys.* **2010**, *12*, 373–381.
- (20) (a) Nakano, M.; Kishi, R.; Nitta, T.; Kubo, T.; Nakasuiji, K.; Kamada, K.; Ohta, K.; Champagne, B.; Botek, E.; Yamaguchi, K. *J. Phys. Chem. A* **2005**, *109*, 885–891. (b) Nakano, M.; Kishi, R.; Ohta, S.; Takahashi, H.; Kubo, T.; Kamada, K.; Ohta, K.; Botek, E.; Champagne, B. *Phys. Rev. Lett.* **2007**, *99*, 033001–1–4. (c) Nakano, M.; Kishi, R.; Ohta, S.; Takebe, A.; Takahashi, H.; Furukawa, S.; Kubo, T.; Morita, Y.; Nakasuiji, K.; Yamaguchi, K.; et al. *J. Chem. Phys.* **2006**, *125*, 074113–1–9. (d) Nakano, M.; Yoneda, K.; Kishi, R.; Takahashi, H.; Kubo, T.; Kamada, K.; Ohta, K.; Botek, E.; Champagne, B. *J. Chem. Phys.* **2009**, *131*, 114316–1–7. (e) Nakano, M.; Champagne, B.; Botek, E.; Ohta, K.; Kamada, K.; Kubo, T. *J. Chem. Phys.* **2010**, *133*, 154302–1–15. (f) Nakano, M.; Minami, T.; Yoneda, K.; Muhammad, S.; Kishi, R.; Shigeta, Y.; Kubo, T.; Rougier, L.; Champagne, B.; Kamada, K.; et al. *J. Phys. Chem. Lett.* **2011**, *2*, 1094–1098.
- (21) (a) Nakano, M.; Kubo, T.; Kamada, K.; Ohta, K.; Kishi, R.; Ohta, S.; Nakagawa, N.; Takahashi, H.; Furukawa, S.; Morita, Y.; et al. *Chem. Phys. Lett.* **2006**, *418*, 142–147. (b) Ohta, S.; Nakano, M.; Kubo, K.; Kamada, K.; Ohta, K.; Kishi, R.; Nakagawa, N.; Champagne, B.; Botek, E.; Takebe, A.; et al. *J. Phys. Chem. A* **2007**, *111*, 3633–3641. (c) Nakano, M.; Kishi, R.; Yoneda, K.; Inoue, Y.; Inui, T.; Shigeta, Y.; Kubo, T.; Champagne, B. *J. Phys. Chem. A* **2011**, *115*, 8767–8777 and references therein.
- (22) (a) Kamada, K.; Ohta, K.; Kubo, T.; Shimizu, A.; Morita, Y.; Nakasuiji, K.; Kishi, R.; Ohta, S.; Furukawa, S.; Takahashi, H. M.; et al. *Angew. Chem., Int. Ed.* **2007**, *46*, 3544–3546. (b) Kishida, H.; Hibino, K.; Nakamura, A.; Kato, D.; Abe, J. *Thin Sol. Films* **2010**, *519*, 1028–1030.
- (23) (a) Park, S.; Ruoff, R. S. *Nat. Nanotechnol.* **2009**, *4*, 217–224. (b) Kim, K. S.; Zhao, Y.; Jang, H.; Lee, S. Y.; Kim, J. M.; Ahn, J. H.; Kim, P.; Choi, J. Y.; Hong, B. H. *Nature* **2009**, *457*, 706–710. (c) Li, X. S.; Cai, W. W.; An, J. H.; Kim, S.; Nah, J.; Yang, D. X.; Piner, R.; Velamakanni, A.; Jung, I.; Tutuc, E.; et al. *Science* **2009**, *324*, 1312–1314.
- (24) Kertesz, M.; Choi, C. H.; Yang, S. *Chem. Rev.* **2005**, *105*, 3448–3481.
- (25) Motomura, S.; Nakano, M.; Fukui, H.; Yoneda, K.; Kubo, T.; Champagne, B.; Carion, R.; Botek, E. *Phys. Chem. Chem. Phys.* **2011**, *13*, 20575–20583.
- (26) (a) Hajgató, B.; Ohno, K. *Chem. Phys. Lett.* **2004**, *385*, 512–518. (b) Hajgató, B.; Deleuze, M. S.; Ohno, K. *Chem.—Eur. J.* **2006**, *12*, 5757–5769.
- (27) (a) Stoll, H.; Savin, A. In *Density Functional Methods in Physics*; Dreizler, R., da Providencia, J., Eds.; Plenum: New York, 1985; pp 177–207. (b) Iikura, H.; Tsuneda, T.; Yanai, T.; Hirao, K. *J. Chem. Phys.* **2001**, *115*, 3540–3544.
- (28) Kishi, R.; Bonness, S.; Yoneda, K.; Takahashi, H.; Nakano, M.; Botek, E.; Champagne, B.; Kubo, T.; Kamada, K.; Ohta, K.; et al. *J. Chem. Phys.* **2010**, *132*, 094107–1–11.
- (29) Sekino, H.; Maeda, Y.; Kamiya, M.; Hirao, K. *J. Chem. Phys.* **2007**, *126*, 014107–1–6.
- (30) Yamanaka, S.; Okumura, M.; Nakano, M.; Yamaguchi, K. *J. Mol. Struct. (THEOCHEM)* **1994**, *310*, 205–209.
- (31) Ruud, K.; Helgaker, T.; Bak, K. L.; Jørgensen, P.; Jensen, H. J. A. *J. Chem. Phys.* **1993**, *99*, 3847–3859.
- (32) Schleyer, P. v. R.; Jiao, H. *Pure Appl. Chem.* **1996**, *68*, 209–218.
- (33) Lazzaretti, P. *Phys. Chem. Chem. Phys.* **2004**, *6*, 217–223.
- (34) Carion, R.; Champagne, B.; Monaco, G.; Zanasi, R.; Pelloni, S.; Lazzaretti, P. *J. Chem. Theor. Comput.* **2010**, *6*, 2002–2018.
- (35) Pelloni, S.; Lazzaretti, P. *J. Phys. Chem. A* **2011**, *115*, 4553–4557.
- (36) Shen, Y. R. *The Principles of Nonlinear Optics*; John Wiley & Sons, Inc.: New York, 1984.
- (37) Cohen, H. D.; Roothaan, C. C. *J. J. Chem. Phys.* **1965**, *43*, S34–S39.
- (38) Nakano, M.; Shigemoto, I.; Yamada, S.; Yamaguchi, K. *J. Chem. Phys.* **1995**, *103*, 4175–4191.
- (39) Frisch, M. J.; et al. *Gaussian 03*, revision C.02; Gaussian, Inc.: Wallingford, CT, 2004.
- (40) Yamaguchi, K.; Jensen, F.; Dorigo, A.; Houk, K. N. *Chem. Phys. Lett.* **1988**, *149*, 537–542.
- (41) Nakano, M.; Minami, T.; Fukui, H.; Yoneda, K.; Shigeta, Y.; Kishi, R.; Champagne, B.; Botek, E. *Chem. Phys. Lett.* **2010**, *501*, 140–145.
- (42) Pollet, R.; Amara, H. *J. Chem. Theory Comput.* **2009**, *5*, 1719–1722.
- (43) Nakano, M.; Minami, T.; Fukui, H.; Kishi, R.; Shigeta, Y.; Champagne, B. *J. Chem. Phys.* **2012**, *136*, 024315–1–7.
- (44) Mondal, R.; Tönshoff, C.; Khon, D.; Neckers, D. C.; Bettinger, H. F. *J. Am. Chem. Soc.* **2009**, *131*, 14281–14289.
- (45) Murata, Y.; Kato, N.; Fujiwara, K.; Komatsu, K. *J. Org. Chem.* **1999**, *64*, 3483–3488.